Title

Profiling the Surfaceome Identifies Therapeutic Targets for Cells with Hyperactive mTORC1 Signaling*

Journal

Molecular & Cellular Proteomics, 19(2)

ISSN

1535-9476

Authors

Wei, Junnian
Leung, Kevin
Truillet, Charles
et al.

Publication Date

2020-02-01

DOI

10.1074/mcp.ra119.001785

Peer reviewed

Profiling the Surfaceome Identifies Therapeutic Targets for Cells with Hyperactive mTORC1 Signaling

Authors

Junnian Wei, Kevin Leung, Charles Truillet, Davide Ruggero, James A. Wells, and Michael J. Evans

Correspondence

jim.wells@ucsf.edu and michael.evans@ucsf.edu

In Brief

SILAC proteomics was applied to isogenic cell lines to identify cell surface proteins upregulated by mTORC1 signaling, which identified the proteases neprilysin and aminopeptidase N as the most highly induced. Validation and functional studies showed that the proliferation of cancer cells with hyperactive mTORC1 are sensitized to neprilysin and aminopeptidase N inhibition. These studies introduce a new paradigm for the treatment of cancer cells driven by mTORC1 that may overcome the well-established limitations of kinase inhibitors.

Graphical Abstract

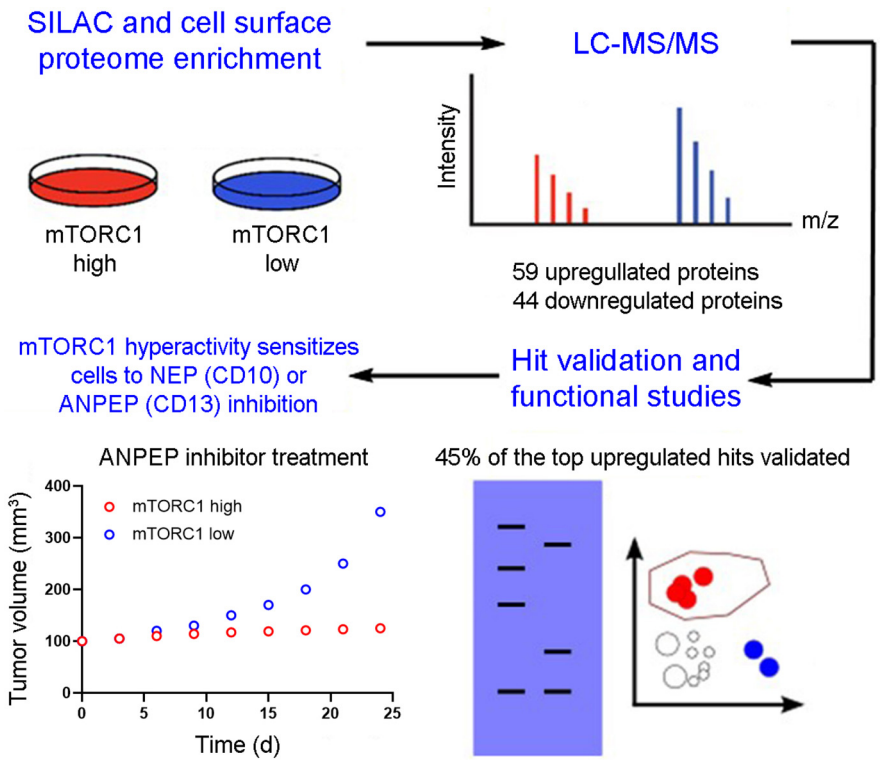

Highlights

- Quantitative proteomes of the cellular surface changes induced by mTORC1 signaling.
- Hit validation in human cancer cell lines and biopsies.
- Functional studies showing new drug targets to which cancer cells with hyperactive mTORC1 may be addicted.
- A new paradigm for drug development, namely targeting cell surface proteins regulated by mTORC1.

Wei et al., 2020, Molecular & Cellular Proteomics *19*, 294–307
February 2020

https://doi.org/10.1074/mcp.RA119.001785

Profiling the Surfaceome Identifies Therapeutic Targets for Cells with Hyperactive mTORC1 Signaling*[S]

Junnian Wei‡¶¶, Kevin Leung§¶¶, Charles Truillet¶, Davide Ruggero‖**, James A. Wells§**‡‡, and Michael J. Evans‡§**§§

Aberrantly high mTORC1 signaling is a known driver of many cancers and human disorders, yet pharmacological inhibition of mTORC1 rarely confers durable clinical responses. To explore alternative therapeutic strategies, herein we conducted a proteomics survey to identify cell surface proteins upregulated by mTORC1. A comparison of the surfaceome from *Tsc1*$^{-/-}$ *versus* *Tsc1*$^{+/+}$ mouse embryonic fibroblasts revealed 59 proteins predicted to be significantly overexpressed in *Tsc1*$^{-/-}$ cells. Further validation of the data in multiple mouse and human cell lines showed that mTORC1 signaling most dramatically induced the expression of the proteases neprilysin (NEP/CD10) and aminopeptidase N (APN/CD13). Functional studies showed that constitutive mTORC1 signaling sensitized cells to genetic ablation of NEP and APN, as well as the biochemical inhibition of APN. In summary, these data show that mTORC1 signaling plays a significant role in the constitution of the surfaceome, which in turn may present novel therapeutic strategies. ***Molecular & Cellular Proteomics 19: 294–307, 2020. DOI: 10.1074/mcp.RA119.001785.***

Because of the importance of mTORC1 to the pathobiology of many cancers and human diseases, there has been longstanding interest in developing therapeutic strategies to inhibit its signaling (1). Over 20 years of research has shown that direct pharmacological inhibition of mTORC1 biochemistry with small molecules that disrupt the complex (*e.g.* rapalogues) or ATP-site directed inhibitors to mTOR generally show encouraging preclinical activity that often does not translate to durable clinical responses. The current state of the art suggests suboptimal clinical responses can reflect cellular adaptation to mTORC1 inhibition through complex feedback mechanisms or dose limiting toxicity (2, 3).

These considerations motivated us to consider molecular profiling studies to probe for other therapeutic strategies. Much of how a cell defines itself and communicates outwardly is dictated by protein expression patterns on the cellular surface. In the case of mTORC1, some evidence already suggests that downstream signaling can alter protein expression at the cell surface. One prominent example is mTORC1 augmentation of glycolysis, which is upregulated in part by elevated GLUT transporter expression on the cell surface via transcriptional activation and vesicle translocation (4). On this basis, we conducted a global survey of the surfaceome to identify proteins induced by mTORC1 signaling.

In designing the proteomics screen, we appreciated that although many genetic lesions within the PI3K/Akt/mTOR signaling axis are known to confer constitutive mTORC1 activity, some events upstream of mTORC1 can activate branching signaling cascades (*e.g.* PTEN inactivation leading to elevated JNK signaling) (5). To steer the proteomic screen toward cell surface events upregulated by mTORC1, we opted to study cell line models isogenic with respect to expression of the TSC1/TSC2 complex. Under normal conditions, TSC1 heterodimerizes with TSC2 to provide protection from ubiquitin mediated degradation (6), whereas TSC2 employs a GTPase activating protein domain to biochemically convert GTP-Rheb to GDP-Rheb (7). As GTP-Rheb is required for the activation of mTORC1, loss of the TSC1/TSC2 complex results in constitutively high mTORC1 signaling. Moreover, somatic or germline genetic mutations that inactivate TSC1 or TSC2 are observed in several deadly cancers (*e.g.* bladder, kidney) and debilitating human disorders (*e.g.* tuberous sclerosis complex, focal cortical dysplasia) (8), underscoring the clinical relevance of studying the biology of cell lines lacking a functional TSC1/2 complex.

From the ‡Department of Radiology and Biomedical Imaging, University of California San Francisco 505 Parnassus Ave, San Francisco California 94143; §Department of Pharmaceutical Chemistry, University of California San Francisco, 505 Parnassus Ave, San Francisco California 94143; ¶Imagerie Moleculaire In Vivo, INSERM, CEA, Univ. Paris Sud, CNRS, Universite Paris Saclay, CEA-Service Hospitalier Frederic Joliot, Orsay France, 94100; ‖Department of Urology, University of California San Francisco, 505 Parnassus Ave, San Francisco California 94143; **Helen Diller Family Comprehensive Cancer Center, University of California San Francisco, 505 Parnassus Ave, San Francisco California 94143

Received September 18, 2019, and in revised form, November 4, 2019
Published, MCP Papers in Press, December 2, 2019, DOI 10.1074/mcp.RA119.001785

By analyzing the surfaceome of *Tsc1*$^{-/-}$ *versus* *Tsc1*$^{+/+}$ mouse embryonic fibroblasts (MEFs)[1], we show that mTORC1 upregulates (and downregulates) the expression of many proteins on the cellular surface. Among them, we show that neprilysin (NEP/CD10) and aminopeptidase N (APN/CD13) are highly upregulated by mTORC1 in mouse and human cell lines of diverse lineage. Moreover, the growth of cells with constitutively active mTORC1 is dependent on the expression of NEP and APN, as well as the biochemical activity of APN. These data represent a first step toward defining alternative therapeutic strategies for the treatment of mTORC1 driven diseases.

MATERIALS AND METHODS

General Methods—*Tsc1*$^{-/-}$ and *Tsc1*$^{+/+}$MEFs were kindly provided by Professor David Kwiatkowski, and were maintained in high-glucose and glutamine containing DMEM supplemented with 10% FBS and 1% penicillin-streptomycin. The human bladder cancer cell lines T24, 5637, RT4, HCV29, and TCCSUP were purchased from ATCC (Manassas, VA) and subcultured according to the manufacturer's recommendations. The human thyroid cancer cell line 8505 C was purchased from Sigma-Aldrich (St. Louis, MO) and subcultured according to the manufacturer's recommendations. The bladder cancer cell line 97–1 was kindly provided by Professor Margaret Knowles, and subcultured in Hams F12 supplemented with 1% FBS, 1× penicillin-streptomycin, 1× insulin-transferrin-selenium, 2 mM glutamine, 1× non-essential amino acids (NEAA) and 1 μg/ml hydrocortisone. The cell lysis of human embryonic stem cell isogenic pairs were kindly provided by Prof. Helen Bateup from UC Berkeley. LBQ657 was purchased from Cayman Chemical (Ann Arbor, MI). Bestatin was purchased from Sigma-Aldrich (Morrisville, NC). CHR2797 was purchased from MedKoo Biosciences. GDC0941 was purchased from LC Laboratories (Woburn, MA). BKM120 was purchased from AdipoGen (Irvine, CA). Doxorubicin, MK-2206 and BYL-719 were purchased from Adooq Biosciences. All small molecule drugs were used without further purification. Antibodies to total Akt, p-Akt (S473), total S6, p-S6 (S235/236), total S6K, p-S6K (T389), APN (CD13) for mouse cells were acquired from Cell Signaling Technologies (Danvers, MA) and used at a 1:1000 dilution. APN (CD13) for human cells were acquired from Proteintech (Rosemont, Il) and used at a 1:1000 dilution. Actin (clone AC-15) was purchased from Sigma Aldrich and used at a 1:5000 dilution. The NEP (CD10) antibody was purchased from Invitrogen (Waltham, MA) and used at a 1:1000 dilution. Primary antibodies and their respective sources for flow cytometry are listed in supplemental Table S1. Rheb and Akt plasmids were obtained from Addgene (Watertown, MA) (#13831 and #9008, respectively). Primers for rtPCR were synthesized by Integrated DNA Technologies (Redwood City, CA), and a full list of primer sequences appear in supplemental Table S2.

SILAC, Membrane Protein Enrichment, and LC-MS/MS—*Tsc1*$^{+/+}$ and *Tsc1*$^{-/-}$ MEFs were cultured in DMEM SILAC media (Thermo Fisher Scientific, Waltham, MA) containing L-[$^{13}C_6$,$^{15}N_2$]lysine and L-[$^{13}C_6$,$^{15}N_4$] arginine (heavy label) (Thermo Fisher Scientific) or L-[$^{12}C_6$,$^{14}N_2$]lysine and L-[$^{12}C_6$,$^{14}N_4$]arginine (light label) for 5 passages to ensure full incorporation of the isotope labeling on cells. Cells were grown to 70% confluence and harvested after 6 h of serum starvation. Cells were mixed at a 1:1 cell count ratio prior to cell surface capture enrichment. Briefly, live cells were treated with a sodium periodate buffer (2 mM $NaPO_4$, PBS pH 6.5) at 4 °C for 20 mins to oxidize terminal sialic acids of glycoproteins. Aldehydes generated by periodate oxidation were then reacted with biocytin hydrazide in a labeling buffer (1 mM biocytin hydrazide (biotium), 10 mM aniline (Sigma), PBS pH 6.5) at 4 °C for 90 mins. Cells were then washed four times in PBS pH 6.5 to remove excess biocytin-hydrazide and flash frozen.

Frozen cell pellets were lysed using RIPA buffer (VWR) with protease inhibitor mixture (Sigma) at 4 °C for 30 mins. Cell lysate was then sonicated, clarified, and incubated with 500 μl of neutravidin agarose slurry (Thermo Fisher Scientific) at 4 °C for 30 mins. The neutravidin beads were then extensively washed with RIPA buffer, high salt buffer (1 M NaCl, PBS pH 7.5), and urea buffer (2 M urea, 50 mM ammonium bicarbonate) to remove nonspecific proteins. Samples were then reduced on-bead with 5 mM TCEP at 55 °C for 30 mins and alkylated with 10 mM iodoacetamide at room temperature for 30 mins. To release bound proteins, we first performed an on-bead digestion using 20 μg trypsin (Promega; Madison, WI) at room temperature overnight to remove any nonspecific protein binders. The neutravidin beads were extensively washed again with RIPA buffer, high salt buffer (1 M NaCl, PBS pH 7.5), and urea buffer (2 M urea, 50 mM ammonium bicarbonate). To release trypsin digested N-glycosylated peptides bound to the neutravidin beads, peptides were released using 2500U PNGase F (New England Biolabs; Ipswich, MA) at 37 °C for 3 h and eluted using a spin column. PNGase F released peptides were then desalted using SOLA HRP SPE column (Thermo Fisher Scientific) using standard protocol, dried, and dissolved in 0.1% formic acid, 2% acetonitrile prior to LC-MS/MS analysis.

Mass Spectrometry Analysis—Approximately 1 μg of peptide mixture was injected to a pre-packed 0.75 mm x 150 mm Acclaimed Pepmap C18 reversed phase column (2 μm pore size, Thermo Fisher Scientific) attached to a Q Exactive Plus (Thermo Fisher Scientific) mass spectrometer. The peptides were separated using the linear gradient of 3–35% solvent B (Solvent A: 0.1% formic acid, solvent B: 80% acetonitrile, 0.1% formic acid) over 120 mins at 300 μl/min. Data were collected in data-dependent mode using a top 20 method with dynamic exclusion of 35 s and a charge exclusion setting that only sample peptides with a charge of 2, 3, or 4. Full (ms1) scans spectrums were collected as profile data with a resolution of 140,000 (at 200 *m/z*), AGC target of 3E6, maximum injection time of 120 ms, and scan range of 400 - 1800 *m/z*. MS-MS scans were collected as centroid data with a resolution of 17,500 (at 200 *m/z*), AGC target of 5E4, maximum injection time of 60 ms with normalized collision energy at 27, and an isolation window of 1.5 *m/z* with an isolation offset of 0.5 *m/z*.

Proteomics Data Processing—Peptide search for each individual dataset was performed using ProteinProspector (v5.13.2) against 16916 mouse proteins (Swiss-prot database, obtained March 5, 2015) with a false discovery rate (FDR) of <1%. Quantitative data analysis was performed using Skyline (University of Washington) software using the ms1 filtering function. Specifically, spectral libraries from forward and reverse SILAC experiments were analyzed together such that ms1 peaks without an explicit peptide ID would be quantified based on aligned peptide retention time. An isotope dot product of at least 0.8 was used to filter for high quality peptide quantification, and a custom report from skyline was then exported for further processing and analysis using R: A language and environment for statistical computing. To ensure stringent quantification of the surface proteome, only peptides with N to D deamidation modification were included for quantification. To estimate the efficiency of surface protein enrichment, over 90% of proteins identified were annotated with "membrane" but not "mitochondrial" or "nuclear" subcellular localization GO term from Uniprot. Forward and reverse SILAC datasets

[1] The abbreviations used are: MEF, mouse embryonic fibroblasts; NEP, neprilysin; APN, aminopeptidase N; ECL, enhanced chemiluminescence.

were then combined and reported as median $\log_2$ enrichment values for *Tsc1*$^{-/-}$ MEFs. For volcano plots, *p* values were generated using Mann-Whitney *U* test. For Gene Set Enrichment Analysis (GSEA), genes were ranked by median $\log_2$ enrichment values and analyzed against a curated mouse version of the MSigDB (http://bioinf.wehi.edu.au/software/MSigDB/) using the fast pre-ranked gene set enrichment analysis (fgsea) package from Bioconductor.

Flow Cytometry—All cell lines were grown in T75 flasks. Cells were washed with phosphate-buffered saline (PBS) and detached from cell culture dishes by 0.04% EDTA in PBS solution, centrifuged and washed with PBS again. Then the cells were fixed by 1% formaldehyde in PBS solution at 4 °C overnight. The cells were washed centrifuged and washed with PBS, and then counted. Cells were resuspended in 3% BSA in PBS solution to a concentration of 0.7 million cells/100 μl. The primary antibodies were added based on the vendor's recommendations. Cells were washed three times with 3% BSA in PBS solution and re-suspended in 200 μl 3% BSA in PBS solution. One microliter secondary antibodies were added and incubated at room temperature for 30 min if the primary antibodies were unconjugated. Cells were washed three times with 3% BSA in PBS solution and re-suspended in 400 μl PBS. Cells were analyzed on BD FACS Calibur flow cytometer.

Immunoblot—Cell pellets were lysed in RIPA buffer with protease and phosphatase inhibitor cocktails (Calbiochem, San Diego, CA) and then resolved using 1D SDS-PAGE. Xenograft tissue was solubilized using mechanical homogenization in T-PER buffer (Thermo Scientific) with protease and phosphatase inhibitors. Protein concentration was determined with a Bradford absorbance assay, and equal amounts of protein (10–30 μg of lysate) were separated by SDS-PAGE, transferred to PVDF membranes, and immunoblotted with specific primary and secondary antibodies. Immunoreactive bands were visualized using enhanced chemiluminescence (ECL) and detected by chemiluminescence with the ECL detection reagents from Thermo Scientific.

Real Time PCR—Cellular RNA was harvested with a RNAeasy mini kit (Qiagen) using a Qiashredder to disrupt cell pellets. The purity and concentration of RNA was quantified using a NanoDrop spectrometer (ThermoScientific), and 1.5 μg of RNA was converted to cDNA with a high capacity cDNA reverse transcription kit (Applied Biosystems, Foster City, CA). Relative changes in mRNA levels were assessed with a Pikoreal rtPCR cycler (Thermo Fisher Scientific). ΔCt was calculated using the respective actin control, and ΔΔCt was calculated by normalizing ΔCt values to that of vehicle control. Data were expressed as $2^{-\Delta\Delta Ct}$. All measurements were performed with at least 4 replicates and are representative of at least three independent experiments.

Cellular Proliferation Studies—Proliferation/viability of cells was detected by using the CellTiter-Glo Luminescent Cell Viability One Solution Assay (Promega). For the drug treatment assay, cells (1×10^3 cells for MEFs and 2×10^3 cells for human cancer cell lines) were plated on 96-well plates and incubated overnight for cell attachment. Cells were then treated for designed days with different drug treatments. All measurements were performed with at least 4 replicates and are representative of at least three independent experiments.

Gene Suppression with shRNA Knockdown or CRISPR/Cas9 Mediated Genetic Knockout—Five pLKO.1 vectors containing discrete shRNA sequences targeting TSC1 were purchased from the MISSION shRNA collection (Sigma Aldrich). The packaging plasmid pSPAX2 and the envelop plasmid pMD2.G were purchased from Addgene. To prepare lentiviral particles, HEK-293FT cells (1.5×10^6) were plated, and after 18 h, the medium was replaced with antibiotic free DMEM media containing 10% FBS. pLKO.1 (2 μg), pSPAX2 (1.8 μg), and pMD2.G (0.6 μg) plasmids were mixed in 70 μl Opti-MEM. In a separate Eppendorf, Lipofectamine 2000 (15 μl) was diluted in 70 μl Opti-MEM. The solutions containing plasmid and Lipofectamine were mixed and added directly to a plate of HEK293 FT cells. After 12 h, the media was replaced with 5 ml of DMEM containing 1% pen/strep, 10% heat inactivated FBS, and 1.1% BSA. The virus containing media was harvested at 24 h, replaced with fresh media, and harvested again at 48 h. The virus was stored at 4 °C or used immediately after filtration through a low-binding protein membrane (0.45 μm). For infection, 0.2×10^6 bladder cancer cell lines were seed into the 10 cm^2 plates overnight for attaching. Then the media was changed to fresh media containing 8 μg/ml of polybrene. After 2 h, 1 ml of virus media was added. After 24 h, the media was replaced with complete media which contained 1 μg/ml puromycin. After selection by puromycin for 2 weeks, the knockdown effects were checked by Western blotting and the cells were stored for future studies. Of the five shRNA sequences assayed, we determined that optimal knockdown was achieved with the following targeting sequence: 5′ CCGGGCACTCTTTCATCGCCTTTATCTCGAGATAAAGGCGATGAAAGAGTGCTTTTTG-3′, clone ID: NM_000368.3–790s21c1, MISSION TRC no: TRCN0000327868.

To achieve CRISPR mediated gene knockout of TSC1 and TSC2 genes in the NIH-3T3 and T24 cell lines, a similar workflow was followed using the same packaging and envelope plasmids. Two targeting sequences were used in the lentiCRISPRv2 plasmid for TSC1 in T24 cell lines (Addgene): 5′-TCAGGCACCATGATGACAGA-3′ (T24 C1) and 5′-CGAGAGGAT GGATAAACGAG-3′ (T24 C2) (9). Two targeting sequences were used in the lentiCRISPRv2 plasmid for TSC2 in T24 cell lines: 5′- CAGAGGGTAACGATGAACAG -3′ (T24 C3) and 5′- GGGTAACGATGAACAGCGGG -3′ (T24 C4). Targeting sequences used in the lentiCRISPRv2 plasmid for TSC1 and TSC2 knockout in NIH-3T3 cell lines were: 5′- GCGCAAGGTGATCCGAGCAGCGG-3′ (TSC1) and 5′- AACAATCGCATCCGAATGA TAGG-3′ (TSC2). The targeting sequences were designed with CHOPCHOP software (10). After puromycin selection of infected cells for 2 weeks, the corresponding cells were then allowed to expand in complete media to confirm the TSC1/TSC2 knockout via immunoblot.

siRNA Transfection—ONTARGET Plus siRNA SMARTpools against *Mme* and *Anpep* were purchased from Dharmacon (Lafayette, CO). A non-targeting SMARTPool siRNA mixture was used as a negative control. Cells were transfected by Lipofectamine® RNAiMAX Transfection Reagent according to the manufacturer's protocol (Thermo Scientific). In brief, for a 24-well plate, 80,000 cells (in 400 μl medium) were plated in each well and incubated overnight for cell attachment. siRNA solutions were prepared Opti-MEM medium. After adding siRNA, the final concentration of siRNA was 40 nM in each well. 72 h after transfection, cells were counted by CellTiter-Glo. mRNA silencing was confirmed in separate wells using rtPCR.

Plasmids Transfection—NIH-3T3 Cells were transfected by Lipofectamine 2000 Transfection Reagent according to the manufacturer's protocol (Thermo Scientific). In brief, for a 10 cm^2 plate, 1 M cells (in 8 ml medium) were plated in each well and incubated overnight for cell attachment. 6 μg plasmids were prepared in 200 μl Opti-MEM medium with 20 μl Lipofectamine 2000 for 15 min and then added into the plate. Seventy-two hours after transfection, cells were collected for immunoblot.

Apoptosis Assay—Apoptosis of cells was detected by using the Caspase-Glo 9 assay (Promega). For detection of caspase activity and apoptosis, cells (2×10^3/well) were plated on 96-well plates and incubated overnight for cell attachment. Cells were then treated with CHR2797 (final concentration: 2 μM) for 3 or 5 days. All measurements were performed with at least 4 replicates and were independently reproduced three times.

Biochemical Assays—Cellular APN activity was measured with a fluorometric aminopeptidase N activity assay kit (BioVision, Milpitas, CA). Viable, intact cells (5×10^5) were dispersed in 90 μl of assay buffer, and the reaction was initiated by the addition of 10× APN

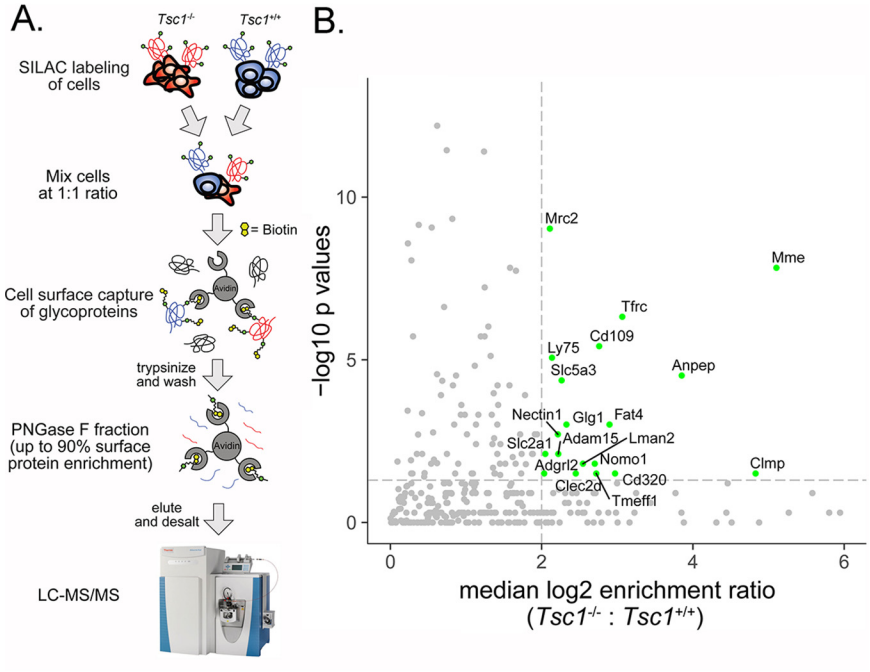

FIG. 1. **Proteomic profiling reveals that mTORC1 signaling remodels the cellular surface.** *A*, A schematic representation of the workflow used to enrich and quantify cell surface proteins in the isogenic pairs of MEFs to enrich and define cell surface proteins up or down-regulated because of TSC1 deletion. *B*, A portion of a volcano plot showing the hits detected in the cell surface proteome of *Tsc1*$^{-/-}$ *versus* *Tsc1*$^{+/+}$ MEFs. The hits labeled in green represent those that had a $\log_2$ fold enrichment > 2 and were statistically significant ($p < 0.05$). Those hits shaded in gray represent proteins detect in the proteomics screen that were not significantly altered.

Substrate solution (10 μl). Substrate hydrolysis by APN was measured at Ex/Em = 384/502 nm every 20 s for 20–45 min at 37 °C. A similar workflow was applied to measure cellular NEP activity using a fluorogenic neprilysin activity assay kit (BioVision) using 1×10^5 cells, the corresponding NEP substrate, and Ex/Em = 330/430 nm. In both cases, the data were plotted using PRISM, and a linear regression was applied to calculate the slope, which represents a rate of substrate hydrolysis proportional to cell surface enzyme expression. The activity was assayed in triplicate, and independently reproduced.

In Vivo Anti-tumor Assessment—All animal studies were performed in accordance with IACUC protocols and were approved by the Laboratory Animal Research Center at UCSF. Intact male *nu/nu* nude mice (Charles River, South San Francisco, CA) received 97–1 or 8505 C cells (1×10^6) in the flank in a 1:1 PBS:matrigel suspension (Corning Matrigel Matrix High Concentration). When tumor volume reached 70–100 mm^3, mice were randomly grouped into arms receiving vehicle (saline) or CHR2797 (100 mg/kg). Intraperitoneal injection was applied and the dose per day for the treatment group was 100 mg/kg in 200 μl formulation (10% DMSO, 10% Tween 80, 80% saline solution). Tumor dimensions were measured with calipers, and the volume was calculated using the following formula: $(mm^3) = (L \times W^2) \times \pi/6$. If any mice lost more than 20% of its weight during the experiments they were euthanized.

Statistical Analysis—Statistical evaluations were performed by Student's *t* test for paired data and by ANOVA for sets of data with multiple comparison points. Data were statistically significant if $p < 0.05$ and labeled in figures accordingly.

RESULTS

SILAC Proteomics Identifies Proteins Differentially Expressed On the Cellular Surface According to TSC1 Status—Isogenic pairs of *Tsc1*$^{-/-}$ and *Tsc1*$^{+/+}$ MEFs were selected for the proteomics screen as the complete genetic knockout of TSC1 would allow for a rigorous binary comparison of proteomic changes because of mTORC1 signaling. A SILAC quantification scheme was coupled to an N-glycan enrichment approach to isolate and analyze cell surface proteomes (Fig. 1*A*) (11, 12). Using these techniques, only glycosylated peptides are captured and analyzed, allowing for high confidence identification and quantification of surface proteins.

Forward and reverse SILAC experiments were performed (light *Tsc1*$^{-/-}$ *versus* heavy *Tsc1*$^{+/+}$, heavy *Tsc1*$^{-/-}$ *versus* light *Tsc1*$^{+/+}$) after 6 h of serum starvation and resulted in quantification of 5197 unique peptide spectra corresponding to 558 cell surface protein IDs. The enrichment ratio (either heavy/light or light/heavy) for each extracellular protein identified was calculated using R and showed strong reproducibility (supplemental Fig. S1*A*–S1*B*). Overall, fifty nine proteins were identified significantly upregulated, and forty four proteins as significantly down regulated in *Tsc1*$^{-/-}$ *versus* *Tsc1*$^{+/+}$ surfaceomes (Fig. 1*B* and supplemental Table S3). Of these, twenty upregulated proteins were predicted to have a median $\log_2$ enrichment ratio ≥ 2 (*Tsc1*$^{-/-}$ *versus* *Tsc1*$^{+/+}$) with $p < 0.05$ (Fig. 1*B*). These included the transferrin receptor and glucose transporter 1, two proteins already known to be induced by mTORC1 (13–15).

To understand if the differentially regulated surface proteins functioned cooperatively, gene set enrichment analysis (GSEA) was applied to the proteomics data. A significant de-enrichment of genes sets associated with focal biological adhesion was identified using a combination of KEGG, REACTOME, BIOCARTA, and HALLMARK gene set libraries (supplemental Fig. S2). The proteins identified on the leading edge of the de-enriched KEGG focal adhesion pathway included *Itga9*, *Itgb3*, *Pdgfra*, *Flt4*, *Egfr*, *Ctnnb1*, *Itga1*, *Erbb3*, *Itga6*, *Mst1r*, and *Itga3*. This finding is consistent with previous literature

A.

Gene	Protein Name	Log_2 ratio
Mme	Neprilysin/CD10	5.10
Anpep	Aminopeptidase N/CD13	3.85
Tfrc	Transferrin receptor	3.07
Cd320	Trancobalamin receptor	2.97
Fat4	Protocadherin Fat 4	2.90
Clec2d	C-type lectin domain family 2 member D	2.45
Glg1	Golgi apparatus protein 1	2.33
Adam15	ADAM15	2.22
Adgrl2	Adhesion G protein-coupled receptor L2	2.03

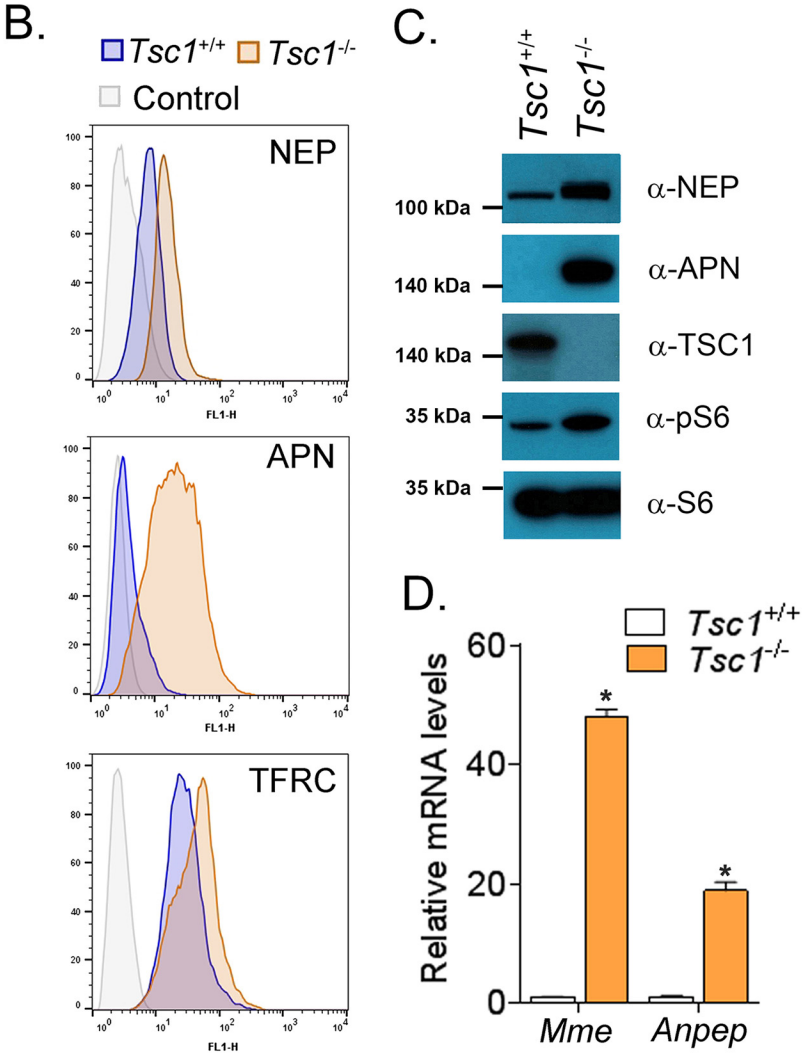

FIG. 2. **Multiple proteins from the proteomics assay validated by hand as upregulated in mouse embryonic fibroblasts.** *A*, A table summarizing the most highly induced hits that validated as significantly induced by flow cytometry in *Tsc1*$^{-/-}$ MEFs. All hits were validated in at least three independent flow cytometry experiments. *B*, Representative histograms from the isogenic MEFs of cell surface NEP, ANPEP and TFRC show the degree of induction because of elevated mTORC1 signaling. Control refers to the signal from cells incubated with secondary antibody alone. *C*, Immunoblot data showing that NEP and APN expression is altered in whole cell lysates of *Tsc1*$^{-/-}$ and *Tsc1*$^{+/+}$ MEFs, in addition to the changes observed on the cellular surface. *D*, Real time PCR data shows that APN and NEP mRNA levels are increased in *Tsc1*$^{-/-}$ MEFs compared with wild type. These data, combined with the expression changes observed in whole cell lysates, suggest that mTORC1 regulates either protease via a transcriptional mechanism. * $p < 0.01$.

showing that the TSC1/TSC2 complex can regulate cellular adhesion (16). GSEA did not identify any significantly enriched gene sets among the proteins predicted to be upregulated in *Tsc1*$^{-/-}$ MEFs.

We next used flow cytometry to validate by hand the top 20 hits predicted to be upregulated on the surface of *Tsc1*$^{-/-}$ MEFs by LC-MS/MS. Nine of the hits were significantly upregulated using commercial polyclonal antibodies (Fig. 2*A*). The most highly upregulated hits by flow were: neprilysin (NEP/CD10, *Mme*), aminopeptidase N (APN/CD13, *Anpep*), the transferrin receptor (TFRC, *Tfrc*), Golgi apparatus protein 1 (GSLG1, *Glg1*), and adhesion G protein coupled receptor L2 (AGRL2, *Adgrl2*, see Fig. 2*B*, supplemental Fig. S3, and supplemental Table S2).

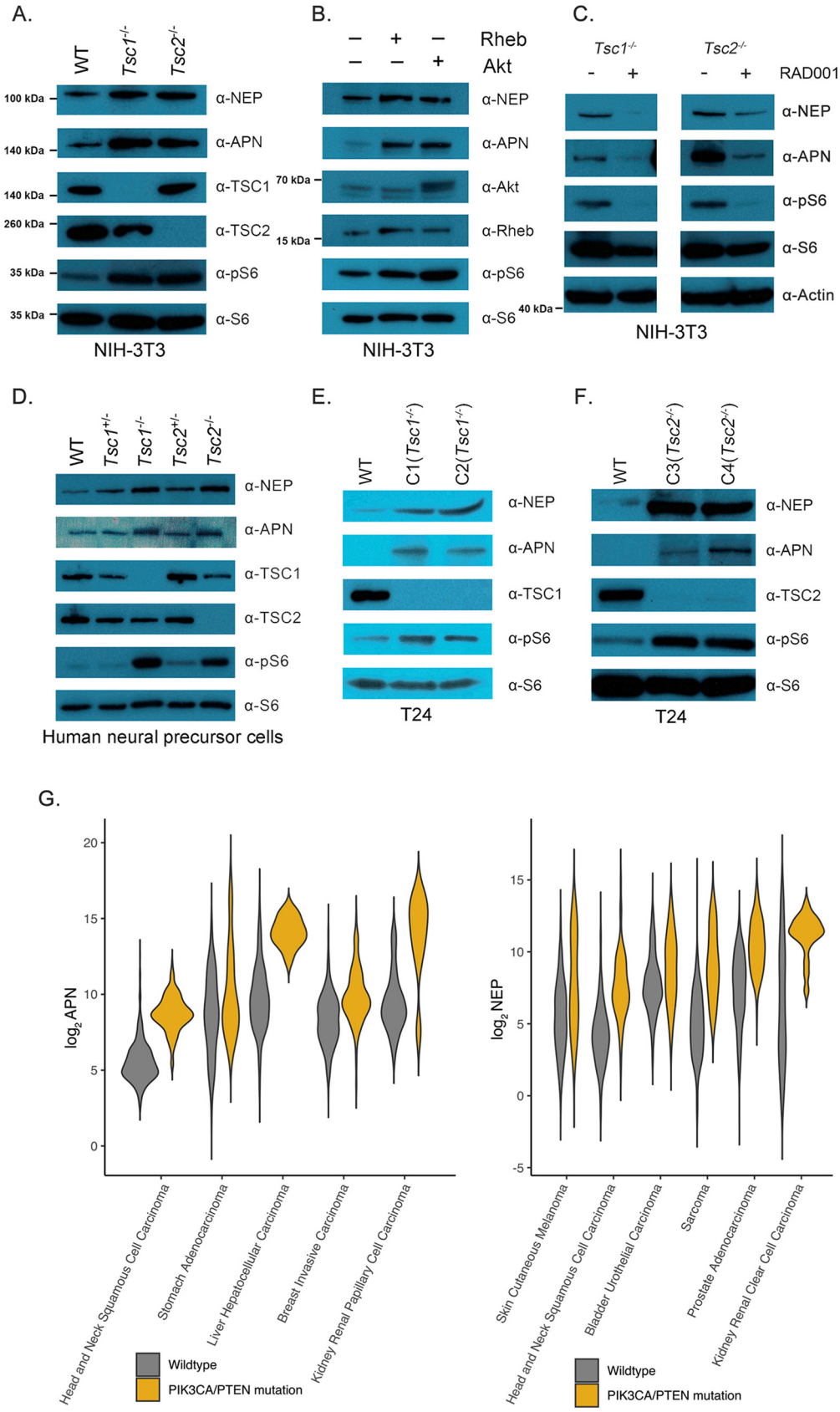
A.
WT
Tsc1-/-
Tsc2-/-
100 kDa
α-NEP
140 kDa
α-APN
140 kDa
α-TSC1
260 kDa
α-TSC2
35 kDa
α-pS6
35 kDa
α-S6
NIH-3T3
B.
Rheb
Akt
α-NEP
α-APN
70 kDa
α-Akt
15 kDa
α-Rheb
α-pS6
40 kDa
α-S6
NIH-3T3
C.
Tsc1-/-
Tsc2-/-
RAD001
α-NEP
α-APN
α-pS6
α-S6
α-Actin
NIH-3T3
D.
WT
Tsc1+/-
Tsc1-/-
Tsc2+/-
Tsc2-/-
α-NEP
α-APN
α-TSC1
α-TSC2
α-pS6
α-S6
Human neural precursor cells
E.
WT
C1(Tsc1-/-)
C2(Tsc1-/-)
α-NEP
α-APN
α-TSC1
α-pS6
α-S6
T24
F.
WT
C3(Tsc2-/-)
C4(Tsc2-/-)
α-NEP
α-APN
α-TSC2
α-pS6
α-S6
T24
G.
log2 APN
Head and Neck Squamous Cell Carcinoma
Stomach Adenocarcinoma
Liver Hepatocellular Carcinoma
Breast Invasive Carcinoma
Kidney Renal Papillary Cell Carcinoma
Wildtype
PIK3CA/PTEN mutation
log2 NEP
Skin Cutaneous Melanoma
Head and Neck Squamous Cell Carcinoma
Bladder Urothelial Carcinoma
Sarcoma
Prostate Adenocarcinoma
Kidney Renal Clear Cell Carcinoma
Wildtype
PIK3CA/PTEN mutation

The Metalloproteases Neprilysin and Aminopeptidase N are Upregulated by mTORC1 Signaling in Phenotypically Diverse Cell Lines—Because NEP and APN were the top upregulated hits, we chose to focus additional studies on these proteases. NEP is a zinc dependent metalloprotease that cleaves peptides at the amino side of hydrophobic residues. In normal physiology, cell surface NEP hydrolyzes peptide-based hormones to inactivate their signaling function (17). APN is a zinc dependent type II metalloprotease that belongs to the M1 family of the MA clan, which can remove the N-terminal amino acids from unsubstituted oligopeptides (18). In normal physiology, APN plays a role in the final digestion of peptides or the processing of peptide-based hormones.

We first tested if NEP and APN were differentially regulated in whole cell lysates of the isogenic MEFs, or if the differential expression levels on the cell surface were caused by a post-translational event. Immunoblot showed that NEP and APN levels were substantially higher in *Tsc1*$^{-/-}$ *versus* *Tsc1*$^{+/+}$ MEFs (Fig. 2*C*). This suggested to us that the mechanism of upregulation may be transcriptional. Consistent with this model, relative mRNA levels of *Mme* and *Anpep* were significantly higher in *Tsc1*$^{-/-}$ compared with *Tsc1*$^{+/+}$ MEFs by rtPCR (Fig. 2*D* and supplemental Fig. S4*A*). These findings are also supported by prior gene expression profiling data (supplemental Fig. S4*B*) (19).

Using the immunoblot assay, we next probed if NEP and APN were upregulated by TSC1 or TSC2 loss in mouse and human cell lines of diverse lineages. Two pairs of NIH-3T3 cells isogenic with respect to TSC1 or TSC2 expression were generated using CRISPR/Cas9 targeted deletion. Reduced TSC1 or TSC2, and elevated mTORC1 signaling was confirmed by immunoblot for phospho-S6. Elevated NEP and APN expression levels were observed in the TSC1 or TSC2 knockout cell lines compare with the parental subline (Fig. 3*A*). This finding motivated us to test if NEP and APN were regulated by mTORC1 activity. We found that NEP and APN expression levels were elevated in NIH-3T3 cells with transient overexpression of myr-Akt or Rheb (Fig. 3*B*). Conversely, treating the TSC1 or TSC2 knockout cell lines with RAD001 reduced NEP and APN expression levels, strongly suggesting mTORC1 regulates the expression of these proteases downstream of TSC1 or TSC2 (Fig. 3*C*).

We next evaluated NEP and APN expression levels in neural precursor cells differentiated from human embryonic stem cells with hetero- or homozygous deletion of TSC1 or TSC2 (20). Immunoblot showed NEP and APN upregulation in the homozygous TSC1 and TSC2 knockout cells compared with the wild-type cell line (Fig. 3*D*). To evaluate the relationship between mTORC1 and the proteases in human cancer cells, we applied CRISPR/Cas9 technology to develop clones of the human bladder cancer cell line T24 with TSC1 knockout (C1, C2) or TSC2 knockout (C3, C4). As expected, the sublines with depleted TSC1 or TSC2 had elevated total NEP and APN expression compared with the parental cell line (Fig. 3*E* and 3*F*). Cell surface NEP or APN expression was also upregulated in T24 or 5637 cells with stable knockdown of TSC1 via shRNA compared with parental cells (supplemental Fig. S5*A*–S5*C*). Last, we tested if elevated NEP and APN expression also resulted in higher biochemical activity in models with hyperactive mTORC1. *In vitro* biochemical assays showed ~2-fold higher biochemical activity in the T24 sublines with both TSC1 and TSC2 deletion compared with wild-type cells (supplemental Fig. S6*A* and S6*B*). Treating the TSC1 or TSC2 null T24 sublines with RAD001 also reduced NEP and APN activity per cell, as expected (supplemental Fig. S6*C*). Collectively, these data suggest that NEP and APN overexpression is mTORC1 dependent in multiple cell lines of diverse species and lineages.

We next asked if NEP and APN mRNA levels are higher in human tumor biopsies harboring mutations known to activate mTORC1 signaling. To address this question, we chose to analyze the TCGA PanCancer data sets. Because TSC1 and TSC2 mutations are rare, the data sets were organized into two groups, (1) samples bearing activating mutations in PIK3CA or those harboring PTEN deletion, or inactivating mutations in PTEN, and (2) all other samples. The relative levels of NEP and APN were then analyzed among the sample groups per data set (*i.e.* per cancer type). As is showing in Fig.

Fig. 3. **NEP and APN expression are upregulated because of mTORC1 signaling in multiple mouse and human cell line models.** *A*, Immunoblot data showing that NEP and APN are upregulated in NIH-3T3 cells with knockout of TSC1 or TSC2 compared with wild-type cells. Knockout sublines were generated using CRISPR/Cas9 deletion. *B*, Immunoblot data showing that NEP and APN are induced in whole cell lysates of NIH-3T3 transiently transfected with myr-Akt or Rheb. The cell lines were harvested 72 h after transfection. *C*, Immunoblot data showing that NEP and APN are downregulated in the whole cell lysates of *Tsc1*$^{-/-}$ or *Tsc2*$^{-/-}$ NIH-3T3 cells by treating with 10 nM RAD001 for 48 h. *D*, Immunoblot data showing that NEP and APN are upregulated in the whole cell lysates of *Tsc1*$^{-/-}$ or *Tsc2*$^{-/-}$ human neuronal precursor cells compare with wild-type (WT) cells. The neuronal precursor cells were differentiated from human embryonic stem cells with the corresponding genotype. *E*, Immunoblot data showing that NEP and APN are induced in two TSC1 knockout sublines (C1, C2) of the human bladder cancer cell line T24 compared with wild type. The TSC1 knockout sublines represent single cell clonal expansions after CRISPR/Cas9 deletion. *F*, Immunoblot data showing that NEP and APN are induced in two TSC2 knockout sublines (C3, C4) of the human bladder cancer cell line T24 compared with wild type. TSC2 was deleted to produce the C3 and C4 sublines with CRISPR/Cas9 technology. *G*, Transcripts of APN and NEP are significantly upregulated in certain cancer types with mTORC1 hyperactivity. Transcript levels for APN and NEP were obtained from TCGA PanCancer study (9892 samples, TCGA Research Network: https://www.cancer.gov/tcga) and cancer types showing significantly upregulation (*t* test *p* value < 0.05) is shown as log2(RSEM) values. In total, 2075 of 9892 samples had at least one occurrence of PI3KCA amplification, H1047, E545, or E552 mutation and PTEN deletion, truncation mutations, and R130 inactivating mutation. Mutational status was obtained from cbioportal.

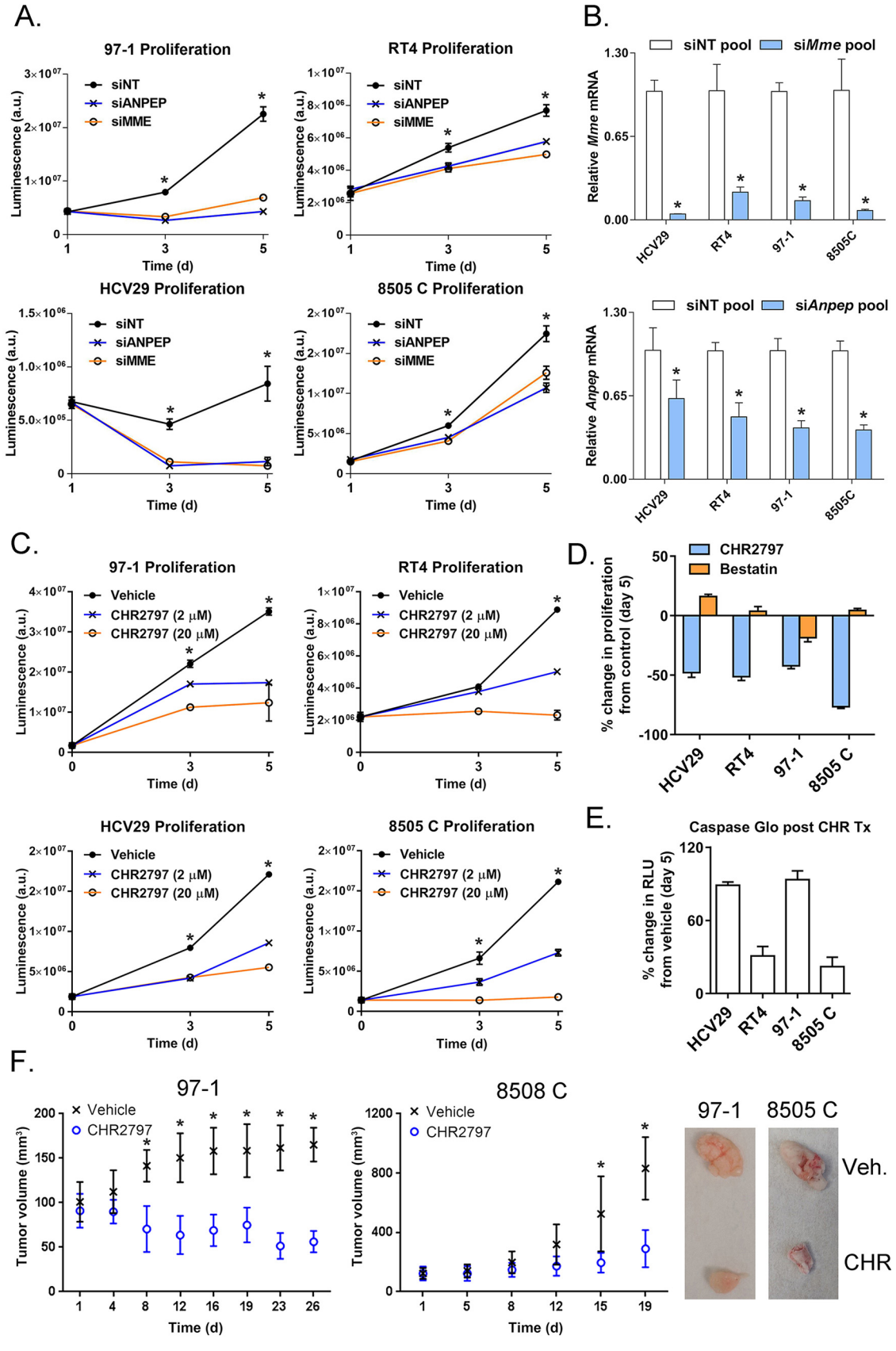
A.
97-1 Proliferation
RT4 Proliferation
HCV29 Proliferation
8505 C Proliferation
siNT
siANPEP
siMME
Luminescence (a.u.)
Time (d)
B.
siNT pool
siMme pool
Relative Mme mRNA
siAnpep pool
Relative Anpep mRNA
HCV29
RT4
97-1
8505C
C.
Vehicle
CHR2797 (2 μM)
CHR2797 (20 μM)
D.
CHR2797
Bestatin
% change in proliferation from control (day 5)
E.
Caspase Glo post CHR Tx
% change in RLU from vehicle (day 5)
F.
97-1
8508 C
Vehicle
CHR2797
Tumor volume (mm3)
Veh.
CHR

3*G*, NEP and APN mRNA levels were found to be higher in sample groups bearing PIK3CA or PTEN mutations for several cancers. Many other cancers showed no statistically significant changes or the reverse trend, which perhaps highlights that the regulation of the proteases by mTORC1 is cell type specific or can be driven by other signaling pathways (supplemental Fig. S7).

Suppression of Neprilysin or Aminopeptidase N Reduces the Proliferation of TSC1 Mutant Cancer Cells—We next tested whether NEP and APN are required for proliferation in cells with constitutive mTORC1 signaling. Four human cancer cell lines with somatic inactivating TSC1 mutations were studied: the bladder cancer cell lines HCV29 (TSC1 Q55X), RT4 (TSC1 L557fs), 97–1 (TSC1 R692X), and the thyroid cancer cell line 8505 C (TSC1 R692Q, see also supplemental Fig. S8*A*). After NEP and APN expression were confirmed in all cell lines via immunoblot (supplemental Fig. S8*B*), we evaluated the effects of NEP or APN knockdown on proliferation using commercial siRNA SMARTpools. Treatment with siRNAs against NEP or APN potently reduced proliferation in all cell lines at 3 and 5 days post transfection compared with treatment with a non-targeting siRNA (Fig. 4*A*). Gene knockdown was confirmed via rtPCR (Fig. 4*B*). To verify the specificity of the antiproliferative effects for NEP or APN knockdown, NEP and APN null cell lines (two cell lines per gene) were treated with the respective siRNA pool. No antiproliferative effects were observed at 3 and 5 days post transfection compared with cells receiving no treatment (supplemental Fig. S8*C*).

We next evaluated if biochemical inhibition of either protease reduced cellular proliferation. We chose to first study CHR2797, a second-generation APN inhibitor with enhanced potency and selectivity compared with bestatin that has shown clinical activity in patients with solid and hematologic cancers (21, 22). Proliferation was not substantially reduced at 1 day post treatment, although a clear antiproliferative effect was observable in all cell lines at 3 and 5 days (Fig. 4*C*). Treating the cells with high doses of the broad-spectrum peptidase inhibitor bestatin did not suppress cellular proliferation at three or 5 days, underscoring the importance of selective and potent APN inhibition to the anti-proliferative effects (Fig. 4*D* and supplemental Fig. S9). CHR2797 also induced caspase 9 activity, showing that APN inhibition can contribute to cell death (Fig. 4*E*). Interestingly, treatment of the cell line panel with the NEP inhibitor LBQ657—the bioactive form of the clinically approved prodrug Sacubitril—did not impact proliferation of the cells at 3 or 5 days (supplemental Fig. S10). The antiproliferative effects of CHR2797 also translated *in vivo*, as the growth of subcutaneous 97–1 and 8505 C tumors were suppressed by daily i.p. CHR2797 treatment over 19–26 days (Fig. 4*F*). Collectively, these data show that mTORC1 upregulates cell surface proteins that can be targeted individually to suppress cell proliferation and viability.

Loss of TSC1 or TSC2 Can Sensitize Cells to the Effects of NEP or APN Ablation, and APN Biochemical Inhibition—We next tested if the antiproliferative effects of siRNA targeting NEP or APN were specific to or enhanced in cells with elevated mTORC1 activity. Although siRNA ablation of NEP or APN resulted in little antiproliferative effects in T24 parental cells (Fig. 5*A*), siRNA significantly reduced the proliferation of TSC1 null C1 and C2 cells (Fig. 5*B* and 5*C*) and TSC2 null C3 and C4 cells (Fig. 5*D* and 5*E*). Expressing the antiproliferation data at day 5 as a percent change compared with cells treated with non-targeting siRNA show clearly that TSC1 and TSC2 null sublines are more sensitized to NEP or APN knockdown compared with wild-type cells (Fig. 5*F*). In all cases, the efficiency of the siRNA knockdown was confirmed by real time PCR, and the knockdown was found to be equivalent between the sublines, or more efficient in wild-type cells (supplemental Fig. S11).

We next tested if the T24 CRISPR knockout sublines were sensitized to treatment with CHR2797. Dosing CHR2797 over several logs of concentration for 3 days showed that the IC_{50} for growth inhibition in both TSC1 and TSC2 knockout cells was significantly lower than the parental T24 (Fig. 6*A*, top). Moreover, treating cells with CHR2797 at 10 μM for 5 days resulted in stronger antiproliferative effects in the TSC1 and TSC2 knockout cells compared with parental T24 (Fig. 6*A*, bottom). We hypothesized that a mechanistic explanation for

Fig. 4. **Functional studies reveal a dependence on NEP and APN for the proliferation and survival of endogenously TSC1 null cancer models.** *A*, Proliferation studies with TSC1 mutant human bladder cancer and thyroid cancer cell lines show that all cell lines are sensitive to siRNA pools targeted to *Mme* and *Anpep*. Data were collected at day 1, 3 and 5 post transfection using the Cell TiterGlo assay, and the luminescence values were plotted alongside those acquired for cells treated with a non-targeting (NT) siRNA pool. *B*, Real time PCR data show that knockdown of *Mme* and *Anpep* is approximately equivalent over the cell line panel. *C*, Proliferation studies with TSC1 mutant human bladder cancer and thyroid cancer cell lines show cells sensitive to a biochemical inhibitor of APN. Treatment with CHR2797 at 2 or 20 μM resulted in potent antiproliferative effects in all cell lines. Cell viability was acquired with the Cell TiterGlo assay after drug exposure for 3 and 5 days. *D*, A comparison of percent changes in cell number after 5 days of incubation with CHR2797 (2 μM) and bestatin (20 μM) shows that potent and specific APN inhibition is required for antiproliferative effects. *E*, Caspase Glo data showing that CHR2797 (2 μM) induces caspase 9 activity after 5 days of drug exposure in all of the TSC1 mutant human cancer cell lines. The data is expressed as a percent change in luminescent signal in CHR2797 treated cells compared with vehicle treated cells. *F*, Treatment of nu/nu mice bearing subcutaneous 97–1 (left) or 8505 C (middle) xenografts with 100 mg/kg CHR2797 suppressed tumor growth over 20–26 days *in vivo* compared with vehicle treated mice (200 μl of saline per mice per day). Treatments were administered once daily via i.p. injection. Photographs of representative tumors surgically excised from mice exposed to CHR2797 (100 mg/kg) or saline. The tumors were obtained at the end of the dosing regimen, and the 97-1 tumors are represented at 4x magnification. * $p < 0.01$.

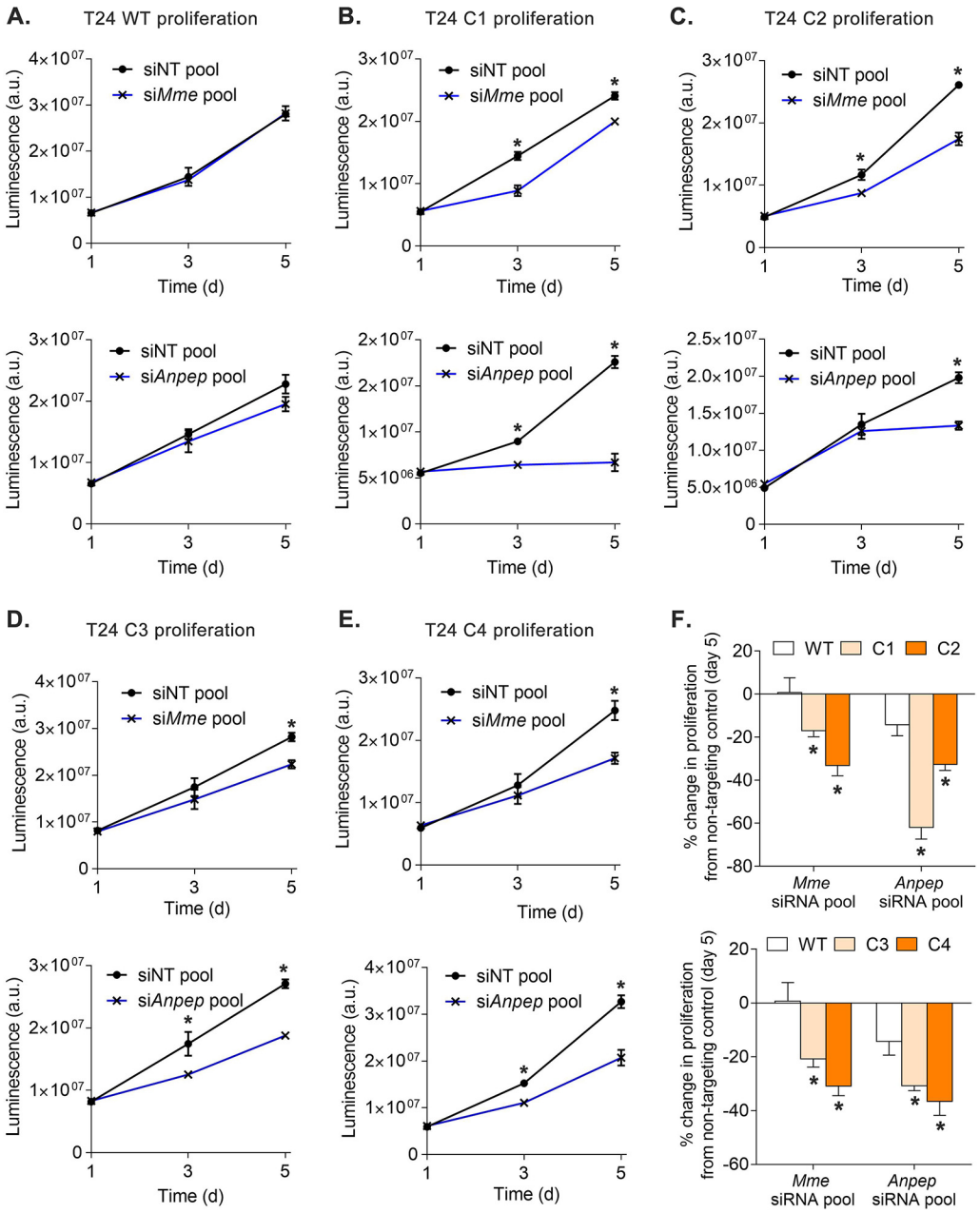

FIG. 5. **Elevated mTORC1 signaling sensitizes cells to genetic ablation of NEP and APN.** *A–E*, Proliferation studies show that suppression of NEP and APN with siRNA results in stronger antiproliferative effects in T24 C1, C2, C3 and C4 than the parental T24. Luminescence data were acquired at day 1, 3 and day 5 post transfection. *F*, The day 5 proliferation data represented as a percent change from non-targeting siRNA pools show that the C1–C4 T24 sublines are significantly more responsive to siRNA pools against *Mme* and *Anpep*. * $p < 0.01$.

the enhanced sensitivity of TSC1 and TSC2 null cells to APN inhibition could be downstream inhibition of mTORC1. We were drawn to this hypothesis as CHR2797 treatment was previously shown to suppress mTORC1 signaling in human cancer cell lines, and recent clinical data have suggested that cancers harboring TSC1 mutations are sensitized to mTORC1 inhibition.(23,24) However, treating 97–1 cells with high doses of CHR2797 had no impact on the phosphorylation levels of mTORC1 substrates in our hands (Fig. 6*B*). Moreover, co-treating cells with CHR2797 and one of several PI3K pathway inhibitors (BKM120, GDC0941, BYL719, or MKK2206) resulted in greater antiproliferative effects than the respective single agents in human TSC1 mutant cell lines. The finding that CHR2797 does not override the antiproliferative effects of the PI3K pathway inhibitors further suggested to us no impact on mTORC1 activity (Fig. 6*C* and supplemental Fig. S12). Lastly, dosing T24 isogenic pairs with BKM120 or GDC0941 showed that the TSC1 and TSC2 knockout sublines were

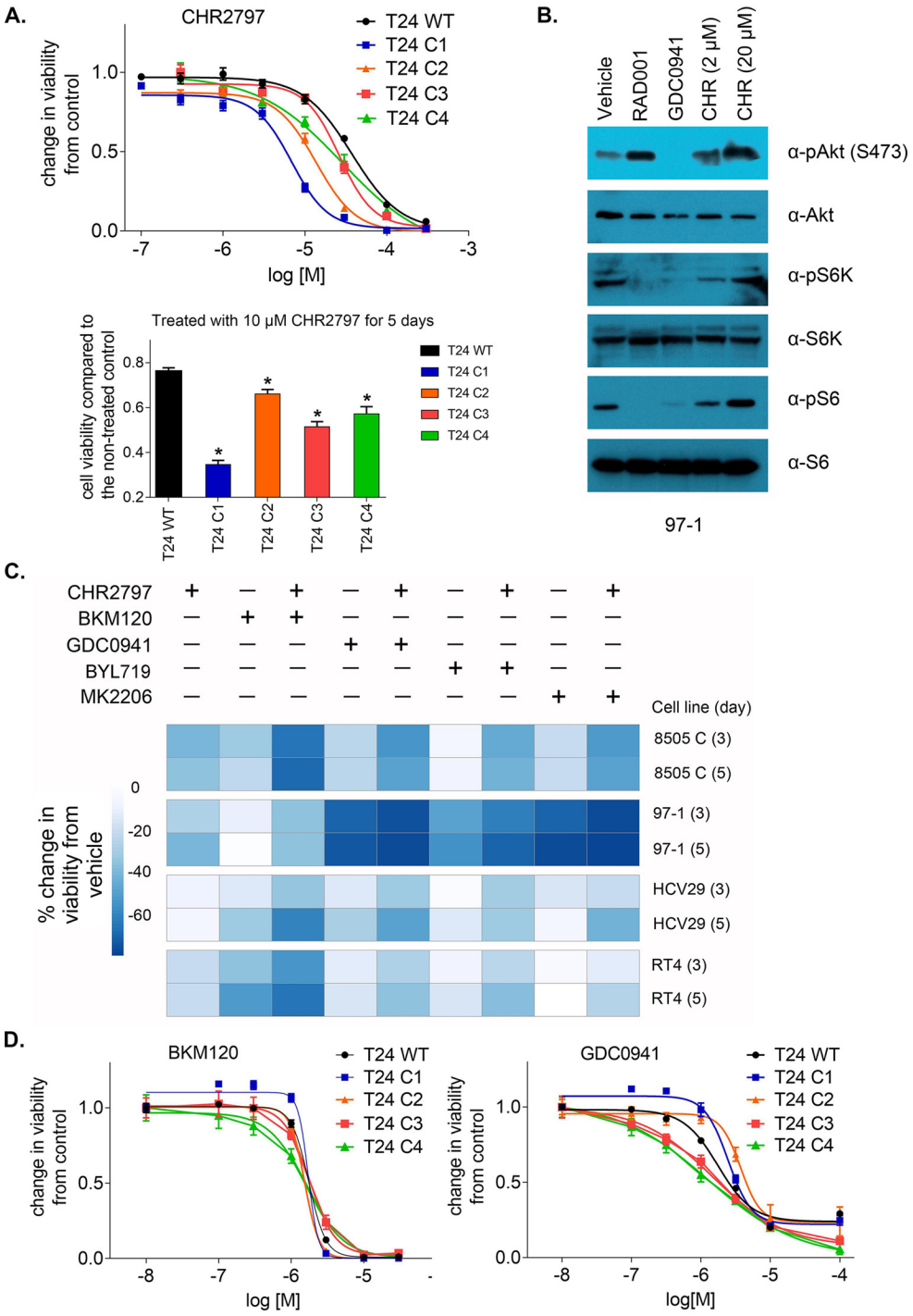

E.

	IC50 (μM)		
Cell line	**CHR2797**	**BKM120**	**GDC0941**
T24	37.4±7.2	1.8±0.1	1.7±0.1
T24 C1	6.9±0.5	1.7±0.1	2.4±0.2
T24 C2	13.7±0.2	1.5±0.1	3.7±1.0
T24 C3	26.3±3.1	1.8±0.2	1.5±0.4
T24 C4	28.8±7.4	1.6±0.2	1.3±0.4

equally sensitive to treatment as the parental subline, which also implied that the enhanced sensitivity of TSC1 null cell lines could not be solely attributed to mTORC1 inhibition (Fig. 6*D* and 6*E*).

DISCUSSION

The purpose of this project was to define new strategies to treat clinically problematic cells characterized by hyperactive mTORC1 signaling. A global proteomics survey revealed that mTORC1 significantly remodels the surfaceome to display potential therapeutic targets like NEP and APN. Validation of the proteomics data suggested that NEP and APN upregulation by mTORC1 may be a common cellular feature, as their induction by mTORC1 was observed in five diverse cell lines of mouse or human origin. Exploratory studies in the TCGA PanCancer data sets also showed that NEP and APN mRNA are upregulated in some cancers with mutations in PIK3CA and/or PTEN compared with tissues with neither mutation. Functional studies showed that cells with elevated mTORC1 signaling are sensitized to genetic or pharmacological inhibition of APN, and genetic ablation of NEP. In summary, this first survey of the cell surface proteomic changes associated with mTORC1 signaling suggest at least two protein targets that might be exploitable to improve the treatment of mTORC1 driven disorders.

Except for the transferrin receptor, the data connecting mTORC1 signaling to the proteins identified from the proteomics screen is generally scant. That said, our review of the literature did reveal several prior observations about APN that we interpret as supportive of our findings. For instance, APN mRNA levels were previously shown to be induced by loss of TSC2 in non-immortalized MEFs (25). APN mRNA levels were also suppressed in *Tsc2*$^{-/-}$ MEFs by RAD001 treatment in the same report, although protein expression changes were not studied. Moreover, APN mRNA levels were higher in TSC2 mutant renal angiomyolipoma biopsies compared with normal kidneys (26).

Our data suggest that mTORC1 may regulate the expression of NEP and APN through transcriptional mechanisms, as mRNA levels of either protease are altered by mTORC1. Although unraveling which transcription factors are involved in NEP or APN regulation may be complicated, several manuscripts have reported that APN expression is induced by RAS in normal or transformed cell lines via Ets-2 transcriptional activation (27, 28). We are currently exploring if RAS induction of APN involves mTORC1, and if mTORC1 activates Ets-2 to induce APN overexpression.

APN overexpression is well documented in many human cancers, and thought to utilize its biochemistry to promote invasion and metastasis (29). Our knockdown data also point to an unappreciated role for APN in cellular proliferation, which should further underscore its importance as a cancer drug target. Although high doses of drug were required to inhibit proliferation, the treatment data with CHR2797 are nevertheless encouraging and argue for additional drug development to identify more potent and specific APN inhibitors. Parenthetically, we feel comfortable attributing the antiproliferative effects of CHR2797 to APN within the context of this study for at least two reasons. First, the other M1 aminopeptidases for which CHR2797 is a potent inhibitor (*e.g.* leucyl aminopeptidase and puromycin-sensitive aminopeptidase) were not differentially regulated or did not appear in the proteomics data set (23). Second, treatment of T24 wild-type cells, a model with virtually no APN expression, did not result in substantial antiproliferative effects. Toward the goal of developing more potent and specific APN inhibitors, we recently developed four highly potent and specific human Fabs against the ectodomain of APN (30). We are currently characterizing these molecules to determine if they suppress APN biochemistry, as well as functionalizing them with cytotoxic payloads for the treatment of mTORC1 hyperactive cells.

The data showing that mTORC1 induces NEP expression is surprising, as its only prior connection to mTORC1 signaling is as an inhibitor of Akt activation. NEP is understood to function as a tumor suppressor by providing a scaffold to which PTEN can bind on the inner layer of the plasma membrane (31). In this regard, it could be possible that mTORC1 may upregulate NEP to reduce PI3K and Akt signaling, perhaps as part of, or alongside, the previously characterized negative feedback loop (32).

That NEP expression, but not NEP biochemistry, is required for cellular proliferation adds to an already complex narrative about this protease's role in cancer. NEP has historically been thought of as a tumor suppressor, although emerging data suggest that NEP can also promote tumor survival and pro-

Fig. 6. **Elevated mTORC1 signaling sensitizes cells to biochemical inhibition of APN.** *A*, (top) Dose response curves showing that TSC1 or TSC2 null T24 sublines are more responsive to treatment with CHR2797 compared with WT cells. The differences between WT and the TSC null sublines are statistically significant. The cells were exposed to drug for 3 days, and cell number was determined with a Cell Titer Glo assay. (bottom) A bar graph showing the relative cell number after a 5 day exposure of CHR2797 at 10 μM. The cell number data were normalized to T24 wild-type cells exposed to vehicle. * $p < 0.01$ *B*, Immunoblot data showing that treatment with CHR2797 does not suppress the phosphorylation of mTORC1 substrates. The effects of RAD001 (10 nM) and GDC0941 (50 nM) on mTORC1 signaling are shown as controls. 97–1 cells were exposed for 6 h with the drugs at the indicated concentration. *C*, A heat map showing the effects of single agent or combination therapy with CHR2797 and mechanistically discrete inhibitors of nodes within the PI3K/Akt/mTOR signaling pathway. In all cases, co-treatment of a kinase inhibitor augments the effects of CHR2797. *D*, Dose response curves showing that the T24 isogenic pairs are equally sensitive to mTORC1 inhibition. *E*, A grid showing the IC50 values derived from the drug dosing studies. The values are reported as mean ± standard deviation, and were calculated from four replicates.

gression. For instance, NEP knockdown with shRNA was recently found to inhibit the proliferation of insulinoma cells, though no mechanism was proposed (33). NEP can also function either as a tumor driver or suppressor within the same cancer type, as was recently demonstrated in colon cancer models (34). Further studies are ongoing to understand the biological consequences of NEP suppression in cells with constitutive mTORC1 signaling.

Aside from the transferrin receptor, other hits from the proteomics data set may yet emerge as attractive therapeutic targets. For instance, GSGL1 and AGRL2 are essentially unstudied as drug or diagnostic targets, and the limited normal tissue expression of the G-coupled protein receptor AGRL2 provides a strong rationale for further analysis of this protein, and further studies are ongoing.

Acknowledgments—We thank Mr. Loc Huynh, Yung-hua Wang, Tony Huynh, and Dr. Sarah Elmes for technical assistance, and Dr. Helen Bateup for graciously providing human neuronal precursor cell lysates.

DATA AVAILABILITY

Proteomics data have been deposited to ProteomeXchange Consortium (proteomecentral.proteomexchange.org) via the MassIVE partner repository (dataset identifier PXD014280).

* M.J.E. was supported by the American Cancer Society (130635-RSG-17-005–01-CCE) and the Tuberous Sclerosis Alliance. C.T. was supported by a postdoctoral fellowship from the Department of Defense Prostate Cancer Research Program (PC151060). K.K.L. was funded by the CIHR Postdoctoral Fellowship Award. J.A.W. was funded by NIH Grants R35GM122451, P41CA196276 and the Chan Zuckerberg Biohub Investigator award program. Research from UCSF reported in this publication was supported in part by the National Cancer Institute of the National Institutes of Health under Award Number P30CA082103. The content is solely the responsibility of the authors and does not necessarily represent the official views of the National Institutes of Health.

[S] This article contains supplemental material. The authors declare that they have no conflicts of interest with the contents of this article.

‡‡ To whom correspondence may be addressed: E-mail: jim.wells@ucsf.edu.

§§ To whom correspondence may be addressed: E-mail: michael.evans@ucsf.edu.

¶¶ These authors contributed equally to this work.

Author contributions: J. Wei and M.J.E. designed research; J. Wei, K.L., and C.T. performed research; J. Wei, K.L., D.R., and M.J.E. analyzed data; J. Wei, K.L., and M.J.E. wrote the paper; D.R. and J. Wells contributed new reagents/analytic tools.

REFERENCES

1. Benjamin, D., Colombi, M., Moroni, C., and Hall, M. N. (2011) Rapamycin passes the torch: a new generation of mTOR inhibitors. *Nat. Rev. Drug Discovery* **10,** 868–880
2. Chandarlapaty, S. (2012) Negative feedback and adaptive resistance to the targeted therapy of cancer. *Cancer Discovery* **2,** 311–319
3. Zheng, Y., and Jiang, Y. (2015) mTOR inhibitors at a glance. *Mol. Cell. Pharmacol.* **7,** 15–20
4. Saxton, R. A., and Sabatini, D. M. (2017) mTOR signaling in growth, metabolism, and disease. *Cell* **168,** 960–976
5. Vivanco, I., Palaskas, N., Tran, C., Finn, S. P., Getz, G., Kennedy, N. J., Jiao, J., Rose, J., Xie, W., Loda, M., Golub, T., Mellinghoff, I. K., Davis, R. J., Wu, H., and Sawyers, C. L. (2007) Identification of the JNK signaling pathway as a functional target of the tumor suppressor PTEN. *Cancer Cell* **11,** 555–569
6. van Slegtenhorst, M., Nellist, M., Nagelkerken, B., Cheadle, J., Snell, R., van den Ouweland, A., Reuser, A., Sampson, J., Halley, D., and van der Sluijs, P. (1998) Interaction between hamartin and tuberin, the TSC1 and TSC2 gene products. *Human Mol. Gen.* **7,** 1053–1057
7. Zhang, Y., Gao, X., Saucedo, L. J., Ru, B., Edgar, B. A., and Pan, D. (2003) Rheb is a direct target of the tuberous sclerosis tumour suppressor proteins. *Nat. Cell Biol.* **5,** 578–581
8. Huang, J., and Manning, B. D. (2008) The TSC1-TSC2 complex: a molecular switchboard controlling cell growth. *Biochem. J.* **412,** 179–190
9. Sanjana, N. E., Shalem, O., and Zhang, F. (2014) Improved vectors and genome-wide libraries for CRISPR screening. *Nat. Methods* **11,** 783–784
10. Labun, K., Montague, T. G., Gagnon, J. A., Thyme, S. B., and Valen, E. (2016) CHOPCHOP v2: a web tool for the next generation of CRISPR genome engineering. *Nucleic Acids Res.* **44,** W272–W276
11. Ong, S. E., and Mann, M. (2006) A practical recipe for stable isotope labeling by amino acids in cell culture (SILAC). *Nat. Protocols* **1,** 2650–2660
12. Wollscheid, B., Bausch-Fluck, D., Henderson, C., O'Brien, R., Bibel, M., Schiess, R., Aebersold, R., and Watts, J. D. (2009) Mass-spectrometric identification and relative quantification of N-linked cell surface glycoproteins. *Nat. Biotechnol.* **27,** 378–386
13. Truillet, C., Cunningham, J. T., Parker, M. F. L., Huynh, L. T., Conn, C. S., Ruggero, D., Lewis, J. S., and Evans, M. J. (2017) Noninvasive measurement of mTORC1 signaling with 89Zr-transferrin. *Clin. Cancer Res.* **23,** 3045–3052
14. Galvez, T., Teruel, M. N., Heo, W. D., Jones, J. T., Kim, M. L., Liou, J., Myers, J. W., and Meyer, T. (2007) siRNA screen of the human signaling proteome identifies the PtdIns(3,4,5)P3-mTOR signaling pathway as a primary regulator of transferrin uptake. *Genome Biol.* **8,** R142
15. Buller, C. L., Loberg, R. D., Fan, M.-H., Zhu, Q., Park, J. L., Vesely, E., Inoki, K., Guan, K.-L., and Brosius, F. C. (2008) A GSK-3/TSC2/mTOR pathway regulates glucose uptake and GLUT1 glucose transporter expression. *Am. J. Physiol. Cell Physiol.* **295,** C836–C843
16. Lamb, R. F., Roy, C., Diefenbach, T. J., Vinters, H. V., Johnson, M. W., Jay, D. G., and Hall, A. (2000) The TSC1 tumour suppressor hamartin regulates cell adhesion through ERM proteins and the GTPase Rho. *Nat. Cell Biol.* **2,** 281–287
17. Bayes-Genis, A., Barallat, J., and Richards, A. M. (2016) A Test in Context: Neprilysin: Function, Inhibition, and Biomarker. *J. Am. College Cardiol.* **68,** 639–653
18. Mina-Osorio, P. (2008) The moonlighting enzyme CD13: old and new functions to target. *Trends Mol. Med.* **14,** 361–371
19. Duvel, K., Yecies, J. L., Menon, S., Raman, P., Lipovsky, A. I., Souza, A. L., Triantafellow, E., Ma, Q., Gorski, R., Cleaver, S., Heiden, M. G. V., MacKeigan, J. P., Finan, P. M., Clish, C. B., Murphy, L. O., and Manning, B. D. (2010) Activation of a metabolic gene regulatory network downstream of mTOR complex 1. *Mol. Cell* **39,** 171–183
20. Blair, J. D., Hockemeyer, D., and Bateup, H. S. (2018) Genetically engineered human cortical spheroid models of tuberous sclerosis. *Nat. Med.* **24,** 1568–1578
21. DiNardo, C. D., and Cortes, J. E. (2014) Tosedostat for the treatment of relapsed and refractory acute myeloid leukemia. *Expert Opinion Investigational Drugs* **23,** 265–272
22. Cortes, J., Feldman, E., Yee, K., Rizzieri, D., Advani, A. S., Charman, A., Spruyt, R., Toal, M., and Kantarjian H. (2013) Two dosing regimens of tosedostat in elderly patients with relapsed or refractory acute myeloid leukaemia (OPAL): a randomised open-label phase 2 study. *Lancet Oncol.* **14,** 354–362
23. Krige, D., Needham, L. A., Bawden, L. J., Flores, N., Farmer, H., Miles, L. E. C., Stone, E., Callaghan, J., Chandler, S., Clark, V. L., Kirwin-Jones, P., Legris, V., Owen, J., Patel, T., Wood, S., Box, G., Laber, D., Odedra, R., Wright, A., Wood, L. M., Eccles, S. A., Bone, E. A., Ayscough, A., and Drummond, A. H. (2008) CHR-2797: an antiproliferative aminopeptidase inhibitor that leads to amino acid deprivation in human leukemic cells. *Cancer Res.* **68,** 6669–6679
24. Iyer, G., Hanrahan, A. J., Milowsky, M. I., Al-Ahmadie, H., Scott, S. N., Janakiraman, M., Pirun, M., Sander, C., Socci, N. D., Ostrovnaya, I.,

Viale, A., Heguy, A., Peng, L., Chan, T. A., Bochner, B., Bajorin, D. F., Berger, M. F., Taylor, B. S., and Solit, D. B. (2012) Genome sequencing identifies a basis for everolimus sensitivity. *Science* **338,** 221

25. Pena-Llopis, S., Vega-Rubin-de-Celis, S., Schwartz, J. C., Wolff, N. C., Tran, T. A. T., Zou, L., Xie, X.-J., Corey, D. R., and Brugarolas, J. (2011) Regulation of TFEB and V-ATPases by mTORC1. *EMBO J.* **30,** 3242–3258
26. Martin, K. R., Zhou, W., Bowman, M. J., Shih, J., Au, K. S., Dittenhafer-Reed, K. E., Sisson, K. A., Koeman, J., Weisenberger, D. J., Cottingham, S. L., DeRoos, S. T., Devinsky, O., Winn, M. E., Cherniack, A. D., Shen, H., Northrup, H., Krueger, D. A., and MacKeigan, J. P. (2017) The genomic landscape of tuberous sclerosis complex. *Nat. Commun.* **8,** 15816
27. Bhagwat, S. V., Petrovic, N., Okamoto, Y., and Shapiro, L. H. (2003) The angiogenic regulator CD13/APN is a transcriptional target of Ras signaling pathways in endothelial morphogenesis. *Blood* **101,** 1818–1826
28. Petrovic, N., Bhagwat, S. V., Ratzan, W. J., Ostrowski, M. C., and Shapiro, L. H. (2003) CD13/APN transcription is induced by RAS/MAPK-mediated phosphorylation of Ets-2 in activated endothelial cells. *J. Biol. Chem.* **278,** 49358–49368
29. Wickstrom, M., Larsson, R., Nygren, P., and Gullbo, J. (2011) Aminopeptidase N (CD13) as a target for cancer chemotherapy. *Cancer Sci.* **102,** 501–508
30. Martinko, A. J., Truillet, C., Julien, O., Diaz, J., Horlbeck, M., Whiteley, G., Blonder, J., Weissman, J., Bandyopadhyay, S., Evans, M., and Wells J. A. (2018) Targeting RAS-driven human cancer cells with antibodies to upregulated and essential cell-surface proteins. *eLife* **7**
31. Sumitomo, M., Iwase, A., Zheng, R., Navarro, D., Kaminetzky, D., Shen, R., Georgescu, M.-M., and Nanus, D. M. (2004) Synergy in tumor suppression by direct interaction of neutral endopeptidase with PTEN. *Cancer Cell* **5,** 67–78
32. O'Reilly, K. E., Rojo, F., She, Q.-B., Solit, D., Mills, G. B., Smith, D., Lane, H., Hofmann, F., Hicklin, D. J., Ludwig, D. L., Baselga, J., and Rosen, N. (2006) mTOR inhibition induces upstream receptor tyrosine kinase signaling and activates Akt. *Cancer Res.* **66,** 1500–1508
33. Feng, Z., Wang, L., Sun, Y., Jiang, Z., Domsic, J., An, C., Xing, B., Tian, J., Liu, X., Metz, D. C., Yang, X., Marmorstein, R., Ma, X., and Hua, X. (2017) Menin and Daxx Interact to Suppress Neuroendocrine Tumors through Epigenetic Control of the Membrane Metallo-Endopeptidase. *Cancer Res.* **77,** 401–411
34. Mizerska-Kowalska, M., Bojarska-Junak, A., Jakubowicz-Gil, J., and Kandefer-Szerszen, M. (2016) Neutral endopeptidase (NEP) is differentially involved in biological activities and cell signaling of colon cancer cell lines derived from various stages of tumor development. *Tumour Biol.* **37,** 13355–13368